Journal of Materials Chemistry B

Biomolecular Detection, Tracking, and Manipulation using a Magnetic-Quantum Dot Platform

Journal:	*Journal of Materials Chemistry B*
Manuscript ID	TB-ART-11-2019-002481.R1
Article Type:	Paper
Date Submitted by the Author:	09-Dec-2019

Complete List of Authors:	Mahajan, Kalpesh; The Ohio State University, William G. Lowrie Department of Chemical and Biomolecular Engineering Ruan, Gang; Nanjing University, Department of Biomedical Engineering, College of Engineering and Applied Sciences; The Ohio State University, William G. Lowrie Department of Chemical and Biomolecular Engineering Vieira, Greg; The Ohio State University, Department of Physics; Rhodes University, Department of Physics Porter, Thomas; The Ohio State University, William G. Lowrie Department of Chemical and Biomolecular Engineering Chalmers, Jeffrey; The Ohio State University, William G. Lowrie Department of Chemical and Biomolecular Engineering Sooryakumar, Ratnasingham; The Ohio State University, Department of Physics Winter, Jessica; The Ohio State University, William G. Lowrie Department of Chemical and Biomolecular Engineering; The Ohio State University, Department of Biomedical Engineering

ARTICLE

Biomolecular Detection, Tracking, and Manipulation using a Magnetic Nanoparticle-Quantum Dot Platform

Received 00th January 20xx,
Accepted 00th January 20xx

DOI: 10.1039/x0xx00000x

Kalpesh D. Mahajan[1,†], Gang Ruan[1,2,†], Greg Vieira[3,4], Thomas Porter[1], Jeffrey J. Chalmers[1], R. Sooryakumar[3], Jessica O. Winter*[1,5]

Fluorescent and magnetic materials play a significant role in biosensor technology, enabling sensitive quantification and separations with applications in diagnostics, purification, quality control, and therapeutics. Here, we present a magneto-fluorescent biosensor/separations platform consisting of quantum dots (QDs) and superparamagnetic iron oxide nanoparticles (SPIONs) that are separately encapsulated in amphiphilic block co-polymer micelles conjugated to DNA or protein (i.e., single-stranded (ss) DNA derived from the mRNA of the tumor suppressor protein p53 or avidin protein). Analytes were detected via an aggregation sandwich assay upon binding of at least 1 QD and 1 SPION-containg micelle to result in a fluorescent/magnetic composite. Multiplexed isolation of protein and DNA biomolecules was demonstrated by using QDs of varying emission wavelength; QD fluorescence intensity could be correlated with analyte concentration. Sequential or parallel biomolecule separation was achieved by adding appropriately functionalized SPION-containing micelles and applying user-controlled magnetic fields via patterned magnetic disks and wires. QD fluorescence was used to continuously visualize analyte separation during this process. This QD/SPION platform is simple to use, demonstrates ~10^{-16} M sensitivity in analyte detection (comparible to competing QD biosensors based on energy transfer) with specificity against 1 and 2 basepair mismatches in DNA detection, molecular separations capability in solutions of ~ 10^{-10} M, and permits simultaneous or paralell, multiplexed separation of protein and DNA. Thus, this versatile platform enables self-assembly-based rapid, sensitive, and specific detection and separation of biomolecules, simultaneously and with real-time visualization. This technology demonstrates potential for nanoscale assembly, biosensing, and bioseparations.

Introduction

Fluorescence and magnetism have long been used for real-time detection and quantification of molecules. Efforts to improve these technologies have typically focused on increasing sensitivity, specificity, and multiplexing capability. Quantum dots (QDs), with their broad absorption cross-section, narrow emission spectra, and photostability, have attracted significant attention for fluorescent labelling applications.[1] For sensing, QDs have been applied using techniques such as Förster resonance energy transfer (FRET),[2] fluorescence ratiometry, electrochemiluminescence, and photo-electrochemistry.[3] Concurrently, superparamagnetic iron oxide nanoparticles (SPIONs) have been applied in imaging, manipulation, and biosensing.[4] For sensing, SPIONs are most commonly used to 1) move and/or concentrate a targeted entity or 2) to detect analytes based on their paramagnetic properties. For both applications, SPION properties are critical features, combined with the magnitude of the magnetic energy gradient and/or detection instrument.[5] For example, analytes can be detected directly via superconducting quantum interference devices (SQUID) analysis of SPION-labelled entities.[6] However, these platforms typically lack multiplexing capability, and are hence unable to perform simultaneous sensing and manipulation operations. Further, the current practical size for individual SPIONs used in these applications is ~ 20 nm[7]. However, many individual, small SPIONs can also be combined into a larger aggregate to achieve an effective increase in magnetic volume.[8]

Recently, several groups have developed multimodal detection probes that combine QDs and SPIONs for simultaneous molecular sensing and manipulation.[9] Detection mechanisms can include QD fluorescence quenching by electron and energy transfer mechanisms or direct fluorescent labelling, whereas magnetic capability is employed for analyte separation. However, many of these schemes employ heterofunctional composite nanoparticles (NPs), such as core-shell structures,[10, 11] which can yield false positive binding events. Such platforms may lack sensitivity and specificity.

Based on our development of polymer micelle-NP encapsulant composite materials, we developed a versatile technology that utilizes SPION and QD micelles and engineered magnetic fields to simultaneously manipulate and track different biomolecules

[1]*William G. Lowrie Department of Chemical and Biomolecular Engineering, The Ohio State University, Columbus, OH, USA.*
[2]*Department of Biomedical Engineering, College of Engineering and Applied Sciences, Nanjing University, China.*
[3]*Department of Physics, The Ohio State University, Columbus, OH, USA.*
[4]*Department of Physics, Rhodes College, Memphis, TN, USA.*
[5]*Department of Biomedical Engineering, The Ohio State University, Columbus, USA.*
†These authors contributed equally to this work.
*Correspondence to: winter.63@osu.edu
Electronic Supplementary Information (ESI) available: Particle tracking movies, correlation between QD micelle cluster size and fluorescence intensity, schematic of patterned magnetic disks and wires, and electromagnet setup. See DOI: 10.1039/x0xx00000x

in parallel. This approach groups together several individual QD or SPION encapsulants, increasing QD fluorescence signal[12] and the cumulative magnetic volume[8]. In this approach, individual micelles containing multiple QDs or SPIONs are conjugated to molecules that detect the analyte, but do not target each other. These micelle "bricks" are thus assembled into hierarchical structures by binding target analyte "mortars" (**Figure 1**), whose size is limited by the available analyte concentration. This approach permits detection via fluorescent signals, measurement of hierarchical structure size, and magnetic quantification, a tri-fold duplication of signals that could be used for internal quality control. Further, unlike approaches that rely on detection alone, this approach permits isolation and quantification of target biomolecules. False positives are reduced by the requirement of both fluroescent and magnetic micelle binding events to register a detection event.

Here, we implemented this scheme to detect model streptavidin protein and p53 DNA analyte molecules via assembly of QD-SPION composite materials. The resulting fluorescent and magnetic structures were transported, manipulated, and separated via user-controlled magnetic fields that acted on SPION constituents, whereas fluorescent QD components permitted analysis and quality control through real-time optical characterization. To determine sensitivity, we compared analyte concentration against a fluorescence standard curve, whereas to measure specificity we examined detection of complimentary DNA vs. DNA with 1 or 2 base pair mismatches. Parallel and sequential separation of different biomolecules was also demonstrated by concurrent or sequential addition of functionalized SPION micelles. Thus, this approach complements existing detection platforms by enabling simultaneous separation and detection, which can be multiplexed to simultaneously detect both proteins and DNA,

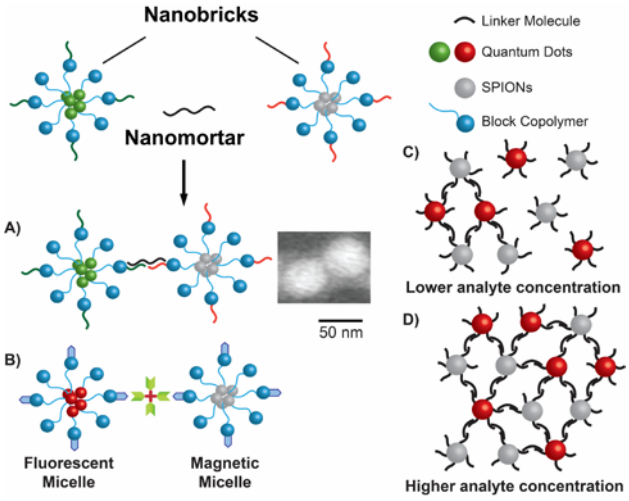

Figure 1. Micelle-Based Aggregation Assay. A detection event occurs when a fluorescent micelle and magnetic micelle both bind to (A) DNA or (B) protein analytes, forming a (C, D) hierarchical material. As analyte concentration increases, additional micelles join the aggregate. Green and red QD micelles were used for ssDNA and protein analytes, respectively.

and provides multiple potential measurement modalities for internal quality control.

Materials and Methods

Materials

Quantum dots supplied in decane (λ_{em} = 545 nm (green), Cat No. Q21791MP and λ_{em} = 605 nm (red), Cat No. Q21701MP), N-(3-Dimethylaminopropyl)-N'-ethylcarbodiimide hydrochloride (EDC) (Cat No. 22980), sulfo-N-hydroxysuccinimide (sulfo-NHS) (Cat No. 24510), and pentyl-amine biotin (Cat No. 21345) were purchased from ThemoFisher Scientific (Waltham, MA). 5nm SPIONs (Cat No. SOR-05-50) were purchased from Ocean NanoTech (San Diego, CA). Carboxyl-terminated poly(styrene-b-ethylene oxide) PS(9500)-b-PEO(18000) (Cat No. P5755-SEOCOOH) was purchased from Polymer Source, Inc. (Dorval, QC, Canada). Poly(vinyl alcohol) (PVA, 13,000-23,000 Dalton, 87-89% hydrolysed, Cat No. 363170), MES buffer (2-(N-morpholino)ethanesulfonic acid (Cat No. M8902), and ssDNA were purchased from Sigma Aldrich (St. Loius, MO). Thiol functionalized methoxy polyethylene glycol (Cat No. MPEG-SH-5000) was purchased from Laysan Bio, Inc (Arab, AL).

Micelle Synthesis

As described previously[12, 13], the interfacial instability approach was used to synthesize micelles containing either QDs or SPIONs. For QDs, stock solutions as supplied by the manufacturer in decane were first transferred to chloroform. QDs (100 µl) were precipitated by adding 450 µl of a 1:2 isopropanol: methanol solution. The pellet was then re-suspended in chloroform to a concentration of 0.1 µM. SPIONs were directly dissolved in chloroform at 3.45 µM. Carboxyl-terminated poly(styrene-b-ethylene oxide) PS(9500)-b-PEO(18000) at 36.4 µM in chloroform was used to encapsulate NPs. The aqueous phase consisted of poly(vinyl alcohol) (PVA) dissolved in water at 5 mg/ml. Micelles were generated by mixing 10 µl polymer solution and 200 µl of QD or SPION solution with 800 µl of the aqueous PVA phase via sonication. Mixtures were left to evaporate for 1-2 hours; formation of a clear, transparent solution indicated successful encapsulation and micelle formation. Micelles can be stable for weeks to months, depending on synthesis conditions[14].

Micelle Bioconjugation

As model systems, biotin was used to capture avidin proteins and p53 DNA was used as a DNA analyte. For avidin protein detection, both QD (red) and SPION micelles were functionalized with biotin. For p53 DNA detection, QD (green) and SPION micelles were functionalized with distinct ssDNA sequences (**Table 1**) that do not bind each other, but hybridize with the same target DNA sequence derived from the mRNA of the tumour suppressor protein p53 (NCBI ref. seq. NM_000546.4). In addition, capture experiments were conducted with single and double mutation sequences to assess

specificity. Mutation locations were chosen randomly, but were excluded from ssDNA locations near NP attachment points.

Table 1. NP and Analyte DNA Sequences

ssDNA	*Sequence*[a]
QD	NH_2C_6-TGAAACGCAAGCCCGA
SPION	CCCTGACCTAACCGCC-C_7NH_2
Target	ACTTTGCGTTCGGGCTGGGACTGGATTGGCGG
1 bp mut.	ACTTTG**T**GTTCGGGCTGGGACTGGATTGGCGG
2 bp mut.	ACTTTG**T**GTTCGGGCTGGGACTGGATTGG**A**GG

[a]Mut. = Mutations, indicated with bold characters. Same colours indicate complimentary sequences.

Micelles were modified with either protein or ssDNA using N-(3-Dimethylaminopropyl)-N'-ethylcarbodiimide hydrochloride (EDC) chemistry.[15] First, carboxylated micelles synthesized in water were re-suspended in pH 5.7 MES buffer. Then, this solution was mixed with EDC, sulfo-NHS, and pentyl-amine biotin or ssDNA at a molar ratio of 1: 1000: 2500: 100 corresponding to micelles: EDC: sulfo-NHS: Biotin or ssDNA. After overnight incubation at room temperature, conjugated micelles were purified by dialysis against distilled, deionized water.

Transmission Electron Microscopy (TEM)

Samples were prepared by placing 10 µL of sample onto a silicone pad. Transfer to formvar/carbon-coated nickel grids was achieved by exposing the grids to the sample droplet for 2 minutes. Samples were negatively stained using phosphotungstic acid (PTA, 1%) by placing the grid on a 10 µl droplet for 2 minutes. Excess PTA was removed with filter paper. Micelles and micellar aggregates were then imaged using an FEI Tecnai G2 Bio Twin TEM.

Dynamic Light Scattering (DLS)

Hydrodynamic particle size was characterized using dynamic light scattering (Brookhaven Instruments Corporation, BI 200SM). Sample concentration was adjusted by addition of water to obtain a scattered light intensity between 10 and 200 kCPS (kilo-counts per second) at a laser wavelength of 633 nm and a detection angle of 90°. Number weighted size was measured for each sample. The size of the micelle composites for each analyte concentration was measured in triplicate, and each replicate was measured three times; the average value was recorded.

Fluorescence Imaging

Samples were imaged using a 100x oil immersion objective on an Olympus IX71 fluorescent microscope. A 100 W mercury lamp was used to generate excitation at λ_{ex} = 488 nm, and a long-pass emission filter was employed to collect emission signal. Images were collected with an Olympus DP70 CCD camera or an EMCCD camera (Photometrics, AZ) with Metamorph software. All image processing and analysis were performed using NIH ImageJ software.

Fluorescence Intensity Quantification and Measurement of Limit of Detection

QD and SPION micelles were used as prepared, at an estimated concentration of 7 x 10^{-10} M. For each experiment, micelles were incubated with analyte (10^{-10} - 10^{-18} M) for ~ 20 min. Then, micelle aggregates were viewed on an Olympus IX71 fluorescence microscope equipped with an Evolve Photometrics EMCCD camera. A stream acquisition of 50 images was recorded for each location, and at least 3 locations were analysed for each concentration. Each fluorescent spot was circled in ImageJ and the total fluorescence intensity was determined. The highest value of total fluorescence intensity among 50 frames was recorded to eliminate interference from QD blinking among constituent particles. This value was compared to that obtained for a single micelle using the same procedure to determine the number of QD micelles bound. The first fluorescence concentration that could be distinguished from that of the control with no analyte was reported as the limit of detection.

Particle Tracking

Hierarchical aggregate trajectories were analysed using MTrackJ plugin[16] available in ImageJ. Particle sizes were obtained from the mean square displacement (MSD) using the Stokes-Einstein equation as described previously.[17] Briefly, the 2D mean squared displacement was calculated by tracking the location of fluorescent aggregates. The diffusion coefficient was then calculated as follows:

$$\boldsymbol{MSD = 4Dt}\ \text{(Equation 1)}$$

where $\boldsymbol{D}$ is the diffusion coefficient, and $\boldsymbol{t}$ is time.[18] Then, the Stokes-Einstein equation was applied to determine particle size:

$$\boldsymbol{D = \frac{k_b T}{3\pi\mu d_p}}\ \text{(Equation 2)}$$

where $\boldsymbol{D}$ is the diffusion coefficient, $\boldsymbol{k_b}$ is Boltzmann's constant, $\boldsymbol{T}$ is the temperature, $\boldsymbol{\mu}$ is the viscosity, and $\boldsymbol{d_p}$ is the particle diameter.

Fabrication of Magnetic Traps

Nano-composites were trapped and manipulated using a nano-scale magnetic platform consisting of patterned wires or disks in the presence of programmable magnetic fields (**Supplementary Figure 1**). The wires and disks were patterned on silicon wafers using electron beam lithography. Two layers of e-beam resist (methylmethacrylate and polymethyl methacrylate) were spin-coated onto the silicon wafer, baked, and exposed to electron beams which draw the desired patterns. Following development, a 40 nm-thick layer of magnetic material was deposited using magnetron sputtering. (The magnetic material used was chosen based on magnetic coercivity. For wires, $Co_{0.5}Fe_{0.5}$ was chosen so that magnetic domains would remain mostly unchanged during experiments, whereas for disks, $Ni_{0.8}Fe_{0.2}$ was chosen so that disk magnetic domains could be easily rotated.) The e-beam resist and excess

magnetic material were lifted off with acetone. The wires (but not disks) were initially magnetized in a desired orientation by applying a temporary ~1 kOe external magnetic field. To minimize surface adhesion and non-specific binding, a 1 nm seed layer of $Ni_{0.8}Fe_{0.2}$ and a 5 nm layer of Au was sputtered atop the entire surface, followed by self-assembly of a thiol-bound PEG monolayer.

Magnetic Manipulation of Particles and Assemblies

The trapping platform consisted of a patterned silicon wafer as well as four electromagnets and one wire coil (**Supplementary Figure 2**). Programmable electrical currents passing through the electromagnets and coil were used to control magnetic fields in three dimensions. The four electromagnets applied field components in the plane of the wafer, whereas the wire coil surrounded the wafer and applied an out-of-plane field component. The out-of-plane field served to strengthen or weaken traps that existed at wire vertices or at the peripheries of disks, whereas the in-plane fields guided the movement of particles manipulated across the silicon wafer.[19] The wafer was placed beneath a 100x oil immersion objective lens in an Olympus microscope, where fluorescence imaging was performed. Images and videos were recorded using an Olympus DP70 CCD camera.

For each experiment, QD and SPION micelles were used as prepared, at an estimated concentration of 7 x 10^{-10} M. Analyte concentration (i.e., 10^{-10} M) was chosen such that the magnetic strength of the micelle aggregates was sufficient to easily manipulate them. Micelles and analytes were incubated together for ~ 20 min. prior to magnetic capture. Three different experiments were performed. In the first experiment, magnetic manipulation of magnetic-fluorescent aggregates formed in the presence of ssDNA analytes was demonstrated on both disk and nanowire platforms to provide proof of concept. In the second experiment, avidin and ssDNA analytes were added together with their respective complementary particles and simultaneous magnetic manipulation of DNA and protein on a nanowire platform was shown. In the third experiment, avidin and ssDNA analytes were added sequentially and sequential manipulation of protein and DNA analytes was shown on a nanowire platform.

Results and Discussion

Hierarchical Assembly of Micelle "Bricks" with Analyte "Mortar"

Multiple QD or SPION NPs were incorporated into individual micelles through the self-assembly of amphiphilic polymers in an aqueous environment.[12, 13] QD micelle sizes were extensively analysed previously.[12] SPION micelles were spherical and ~40 nm in diameter (i.e., 42 ± 13 nm) as confirmed by DLS and transmission electron microscopy TEM (**Figure 2**), consistent with sizes of QD micelles. This approach overcomes some limitations of using individual SPIONs by aggregating multiple SPIONs together to increase overall magnetic volume and therefore magnetic susceptibility.

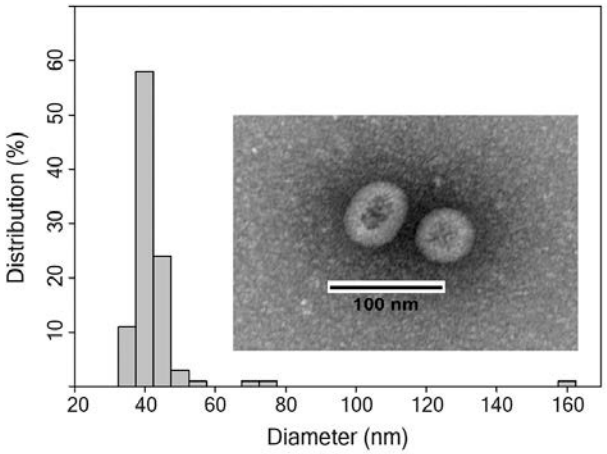

Figure 2. Dynamic light scattering (DLS) and transmission electron microscopy (TEM) analysis of SPION micelle size indicated an average size of 42 ± 13 nm, similar to that of QD micelles.

Individual micelle "nano-bricks" were assembled into hierarchical structures using analyte "nano-mortars" comprised of avidin proteins or ssDNA derived from the p53 mRNA sequence. These hierarchical structures, containing both fluorescent QD and magnetic SPION micelles (e.g., **Figure 1** schematic) were ~50-200 nm in diameter. Using ssDNA analytes for proof of concept, aggregate size and fluorescence intensity were demonstrated to be dependent on the concentration of the analyte mortar (**Figure 3**). QD fluorescence intensity was correlated with aggregate size as measured via aggregate particle tracking, and few aggregates > 100 nm were observed (**Supplementary Figure 3)**. At micelle concentrations of ~ 10^{-10} M, nanoassemblies could be formed in solutions as dilute as 10^{-16} M (i.e., 0.1 fM) (i.e., fluorescence limit of detection), which is improved compared to similar magnetic aggregation assays

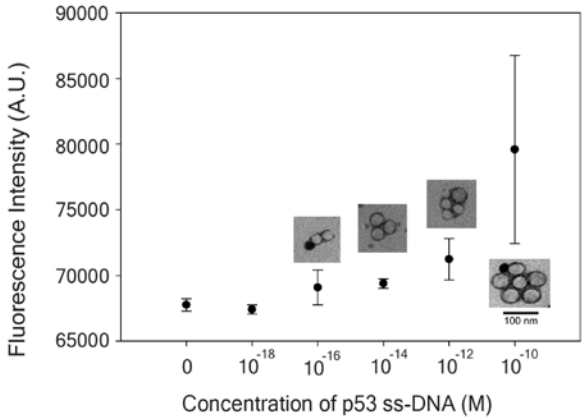

Figure 3. Nanoassembly size increases with increasing target biomolecule concentration (i.e., "nanomortar", here, p53 single stranded DNA). Insets: Representative TEM images of nanoassemblies at the corresponding concentrations of p53 single stranded DNA. (Micelle concentration ~ 7 x 10^{-10} M)

(e.g., 100 pM[20]). These results are also consistent with state-of-the art QD assays that, unlike our aggregation-based system, are based on Förster Resonance Energy Transfer (FRET) (e.g., ~ fM[21]).

Magnetic Collection of Assemblies and Analyte Detection

The proposed approach permits not only detection, but also magnetic isolation of analytes through the use of user-controlled magnetic fields. Engineered magnetic gradients[13, 19] exerted forces on nanoassembly constituent SPIONs to generate motion in a desired direction. Controlled motions across a surface were the result of adding a tuneable, weak electromagnetic field to the strong, arrayed magnetic field gradients of a micro-patterned magnet chip.[13, 19] As an example, assembly circular motion was induced using micropatterned magnetic disk arrays (**Figure 4A**, **Movie S1**), and translational motion was induced via vertex-to-vertex hopping along micropatterned magnetic zigzag wires (**Figure 4B**, **Movie S2**). Typically, ~85% of the fluorescent spots trapped at magnetic vertices (e.g., hybridized nanoassemblies) responded to the modulation of the tunable weak electromagnetic field by moving with similar velocity vectors. Nanoassemblies that did not move in a synchronized fashion were most likely agitated by occasional liquid flow. Although not investigated here, this suggests that liquid flow could also be exploited to provide additional transport modalities through microfluidics, potentially permitting platform integration with existing lab-on-a-chip devices.

Key to this approach is the ability to tune the electromagnetic field via user input, with simultaneous optical readout (via QD fluorescence) of the assembly response. In contrast to manipulation approaches based on scanning probe microscopy[22] and synthetic chemistry[23], the strong and stable fluorescence of QDs[24] enables direct visualization and detection of nanoassembly motion in situ with a fluorescence microscope. The ability to visualize transport and assembly directly also provides a method of quality control in detection. For example, positive detection events required both QD fluorescence and magnetic mobility to indicate nanoassembly formation and thus analyte detection.

These properties were used to assess the sensitivity and specificity of the process. Assemblies that underwent motion in a magnetic field could be characterized via their fluorescence intensity. As a first experiment, ssDNA analyte assemblies were tracked via their fluorescence (**Figure 1A**). As analyte concentration was increased, assembly size and fluorescence intensity increased (**Figure 1C, Figure 1D, Figure 3**). Reliable assembly of clusters ranged from 2 to 27 micelles in solutions containing ~300-1000 biomolecules in the 5 µl samples used in

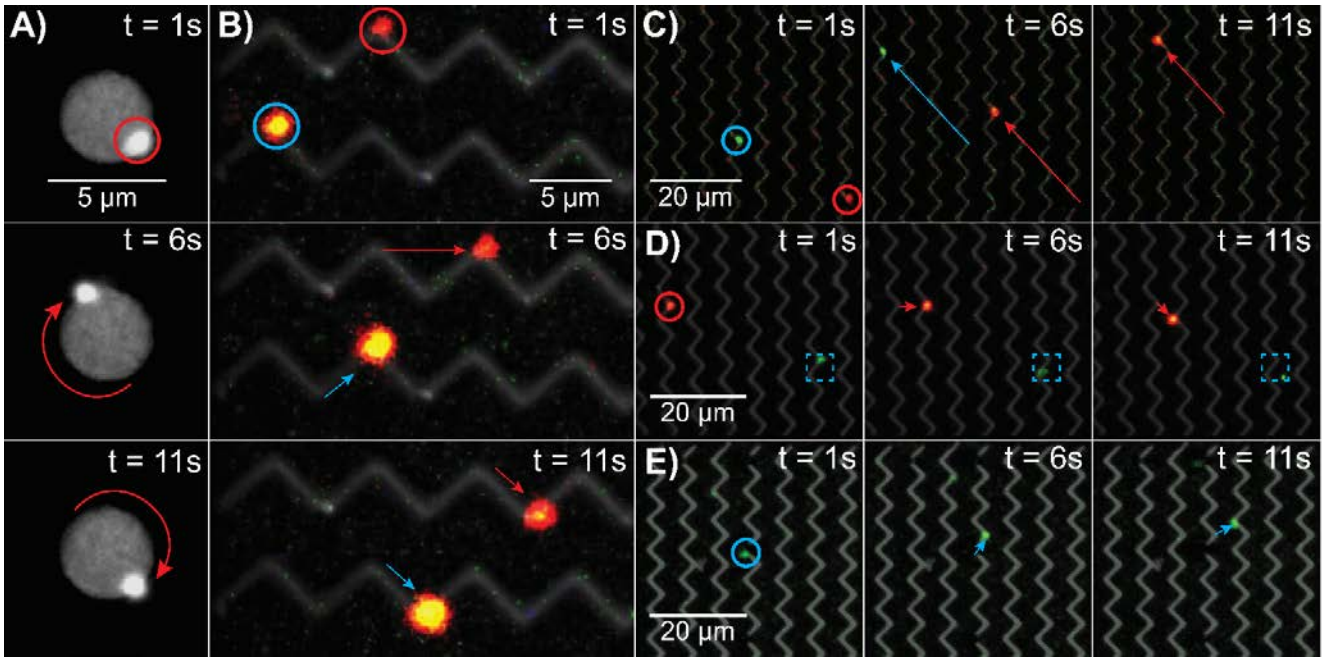

Figure 4. Trapping, transport, and manipulation of composite nanoassemblies (A) on micro-disks, (B) micro-wires, and (C-E) with multiplexing (i.e., still frame images from Supplementary Movies 1-5). In (A) and (B), fluorescent-magnetic nanoassemblies (molecular target: p53 ssDNA, 10^{-10} M) moved around micro-disks and between zigzag micro-wires, respectively, via investigator-controlled modulation of the magnetic field. (C) Red avidin protein (10^{-10} M) and green p53 DNA (10^{-10} M) nanoassemblies were simultaneously transported via investigator-controlled vertex-to-vertex hopping. (D, E) Sequential separation of protein and DNA-based nanoassemblies. (D) Red, magnetic avidin protein nanoassemblies were transported via investigator-controlled vertex-to-vertex hopping, whereas green, non-magnetic p53 DNA nanoassemblies (lacking the magnetic SPION component) moved only as a result of Brownian motion or liquid flow. (E) Green, magnetic p53 DNA nanoassemblies were then formed on the same sample by the addition of complimentary DNA-SPIONs, which were transported via investigator-controlled vertex-to-vertex hopping. The arrows in (A-E) indicate movement of nanoassemblies from the previous frame and are color-coded to represent distinct assemblies.

this study. Biomolecular detection was achieved without any amplification steps (e.g., polymerase chain reaction), and benefitted from the significant signal amplification arising from multiple QDs encapsulated in each QD micelle. Although future work should investigate random sequences and sensitivity of avidin detection in complex solutions containing additional proteins, no detection event (i.e., magnetic motion and corresponding fluorescent signal) was recorded for a 32-nucleotide sequence (i.e., p53 ssDNA) with double or single base pair mismatches (**Table 1**). The high sensitivity and specificity achieved with this small sample volume may be attributed to combining the strong local magnetic field gradients of micro-patterned arrays, which permit isolation of small numbers of biomolecules, and the high fluorescence intensity of constituent QDs, which provide quantitative read-out, into an integrated system.

Multiplexed Collection of Protein and DNA Analytes

This approach also permits simultaneous isolation of both protein and DNA on the same platform. Because constituent QDs exhibit size-dependent fluorescence, a large absorption cross-section, and broad excitation spectra[24], nanoassemblies may be color-coded and their motion simultaneously observed with a single filter set.[13] Color-coded QD-SPION nanoassemblies containing either avidin (red, $\lambda_{emission}$ = 605 nm) or p53 ssDNA (green, $\lambda_{emission}$ = 545 nm) mortars were generated. Red protein and green DNA nanoassemblies were co-transported via investigator-controlled, vertex-to-vertex motions, confirming the ability of this technology to manipulate two types of molecular targets simultaneously (**Figure 4C**, **Figure 5A, Movie S3**). These experiments demonstrate that the intrinsic photoluminescent properties of the QD element may be used to visualize multiplexed control of materials transport. In contrast, observation of rapid, dynamic events using molecular dyes would be infeasible because of the time required to collect and superimpose multiple images from separate colour channels.

In addition to simultaneous transport, specific molecules can also be separated from each other. The feasibility of multiplexed separation with simultaneous visualization was confirmed by separating protein and DNA on the same platform. Here, nanoassemblies were sequentially separated using the micro-patterned magnet array (zigzag wire formation) following addition of the complementary SPION-micelle conjugate (i.e., biotinylated-SPION micelles for avidin protein and p53 ssDNA-SPION micelles for p53 DNA). After a short incubation period (~10-30 min), red QD-avidin-SPION nanoassemblies were transported across a distance of 20 µm via investigator-controlled vertex-to-vertex hopping, whereas green QD-p53 DNA-nanoassemblies (containing no magnetic SPION component) remained near their original location, as their motion was subject only to thermal fluctuations, and not magnetic forces from the wires (**Figure 4D**, **Figure 5B, Movie S4**).

Some movement resulting from Brownian motion and occasional liquid flow was observed in green p53 DNA composites, which was clearly distinguishable from vertex-to-

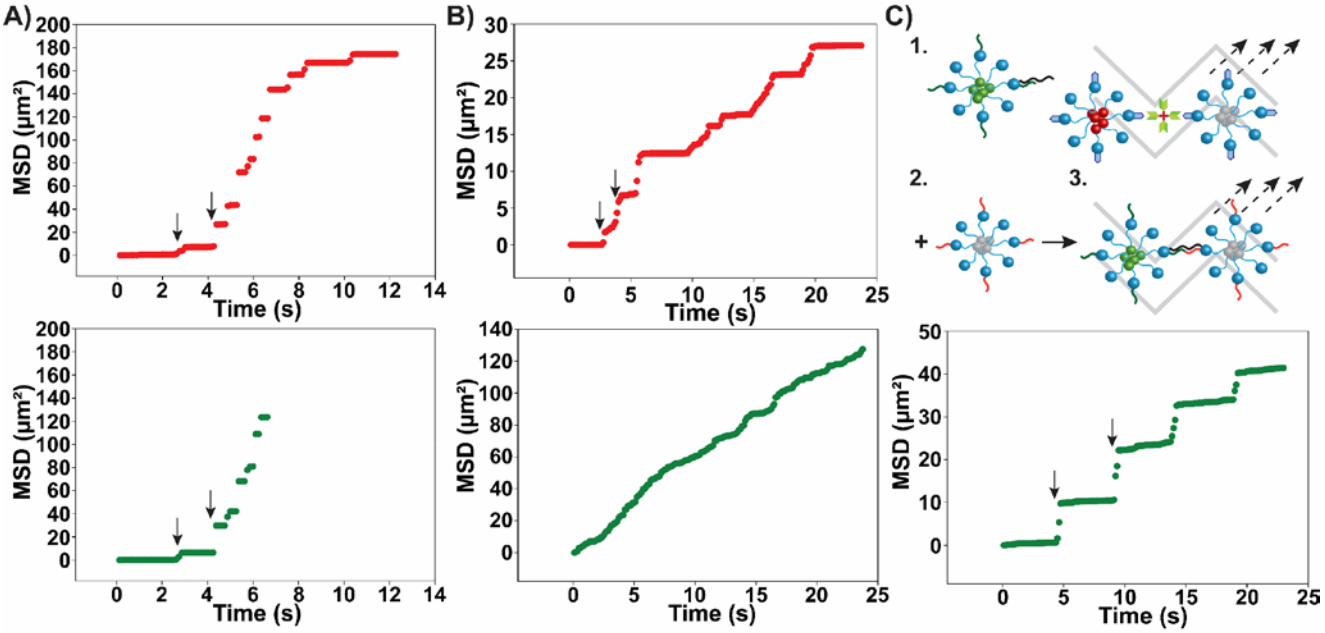

Figure 5. Mean squared displacement (MSD) vs. time for protein (red, upper panel) and DNA (green, lower panel) nanoassemblies. Representative arrows in panels indicate points at which MSD vs. time deviates from the linear trends expected from diffusion alone as a result of vertex-to-vertex hopping induced by user-controlled magnetic fields. Panels A, B, and C correspond to analysis of Figures 4C, D, and E, respectively. (A) Simultaneous transport of protein and DNA assemblies (upper and lower panels) is indicated by deviations from linear MSD (arrows). (B) Sequential magnetic transport of protein assemblies in the presence of DNA assemblies that are not transported is indicated by deviations from linear MSD in the red (upper), but not green (lower) panels. (C) However, when complementary SPIONs are added to green assemblies (lower panel), deviations are restored. Schematic (upper panel) in (C) depicts the process of sequential separation of protein and DNA assemblies.

vertex hopping. Vertex-to-vertex movement by user-controlled magnetic fields was differentiated from movement by diffusion by plotting mean squared displacement (MSD) against time (**Figure 5B**). MSD vs. time behaviour is linear for assemblies undergoing Brownian motion alone (**Equation 1)**. In contrast, assemblies undergoing magnetic transport exhibited deviations from linearity during magnetic trapping events at wire vertices. Thus, the motion of assemblies containing only QDs could be clearly distinguished from the motion of assemblies containing both QDs and SPIONs.

Trapping and transport of the red QD-avidin-SPION nanoassemblies (and the lack of trapping and transport for the green assemblies) was confirmed using the color-coded fluorescence signals, suggesting feasibility of one-component separation from a mixed solution. An aqueous solution of p53 ssDNA-SPION-micelles was then added to create green QD-p53-SPION nanoassemblies. Following incubation (~10-30 min), these assemblies were transported similarly to avidin-assemblies using investigator-controlled vertex-to-vertex motion, (**Figure 4E**, **Figure 5C, Movie S5**), thus demonstrating feasibility of separation of different molecules/assemblies from the same solution. Whereas a number of competing technologies also use color-coded signals to identify many different molecules (e.g., Nanostring[25] or Western blots), this approach has the ability to identify and selectively transport and separate different molecules/assemblies. This result is enabled by the sandwich structure (**Figure 1**) employed for fluorescent-magnetic nanocomposite formation, which takes advantage of the specificity of biomolecular assemblies. Manipulation of analytes at lower concentrations may be feasible by increasing the magnetic strength of the particles[8]. Further, detection speed (i.e., 20 min incubation time) could be reduced by increasing the excess concentration of micelles employed to accelerate binding kinetics.

Conclusions

In this proof of concept work, we demonstrated a magneto-fluorescent detection/ separation platform that (1) performs rapid, sensitive, and specific separation of DNA and/or protein from a 5 µl solution (Speed: Minutes, Limit of Detection: ~0.1 fM via fluorescence, < 0.1 nM via magnetic capture; Sensitivity: No signal for single and double basepair DNA mutations), (2) continuously visualizes individual molecular separation trajectories, and (3) enables multiplexed imaging and separation of analytes. This approach thus permits hierarchical assembly of structures, with the ability to transport, manipulate, and capture those assemblies in an integrated, parallel, and multiplexed manner. In contrast to force microscopy approaches, individual components are combined using a programmable self-assembly method that does not require external intervention or sequential placement to generate higher-order structures. Thus, directional changes can be induced non-invasively. For future applications, these results should be validated in more complex media, using clinical samples and guidelines. This technology could also be enhanced by incorporation of microfluidics for more sophisticated control of flow on the magnetic arrays and to enable future integration with existing lab-on-a-chip technologies. Thus, this technology platform may enable new opportunities in nanoassembly, molecular separation and analysis, and biomolecular research.

Conflicts of interest

JOW/GR are equity holders of Core Quantum Technologies, a company that is commercializing QD and QD/SPION micelles for biomedical applications. This work preceded the founding of that company, which played no role in the experiments described herein.

Acknowledgements

The authors gratefully acknowledge the support of the National Science Foundation, grant numbers: CMMI-0900377, DMR-1206745, EEC-0914790, DMR-0820414; the U.S. Army Research Office under Contract W911NF-10-1-053; the Ohio State University Nanoscale Science and Engineering Center for Affordable Nanoengineering of Polymeric Biomedical Devices, Materials Science and Engineering Research Center for Emergent Materials, and the Institute for Materials Research; a “Thousand Young Global Talents” award from the Chinese Central Government; Nanjing University; and the “Tian-Di” Foundation, College of Modern Engineering and Applied Sciences, Nanjing University, China.

References

1. X. Gao, W. C. Chan and S. Nie, *J. Biomed. Opt.*, 2002, **7**, 532-537.
2. A. R. Clapp, I. L. Medintz, J. M. Mauro, B. R. Fisher, M. G. Bawendi and H. Mattoussi, *J. Am. Chem. Soc.*, 2004, **126**, 301-310.
3. P. Wu, X. Hou, J.-J. Xu and H.-Y. Chen, *Nanoscale*, 2016, **8**, 8427-8442.
4. L. Gloag, M. Mehdipour, D. Chen, R. D. Tilley and J. J. Gooding, *Adv. Mater.*, **0**, 1904385.
5. M. Fratzl, S. Delshadi, T. Devillers, F. Bruckert, O. Cugat, N. M. Dempsey and G. Blaire, *Journal*, 2018, **14**, 2671-2681.
6. J. Wang, H. Li, E. Y. Cho, J. C. LeFebvere and S. A. Cybart, *Ieee Transactions on Applied Superconductivity*, 2019, **29**.
7. S. P. Yeap, S. S. Leong, A. L. Ahmad, B. S. Ooi and J. Lim, *The Journal of Physical Chemistry C*, 2014, **118**, 24042-24054.
8. G. M. Nabar, J. O. Winter and B. E. Wyslouzil, *Soft Matter*, 2018, **14**, 3324-3335.
9. G. Rong, E. E. Tuttle, A. Neal Reilly and H. A. Clark, *Annu. Rev. Anal. Chem.*, 2019, **12**, 109-128.
10. L. Li, C. Jia, F. Wang, H. Fan, W. Jiao and Z. Shao, *Journal of Materials Chemistry C*, 2018, **6**, 2360-2369.
11. L. Wu, Z. Z. Lin, J. Zeng, H. P. Zhong, X. M. Chen and Z. Y. Huang, *Spectrochim Acta A Mol Biomol Spectrosc*, 2018, **196**, 117-122.
12. G. Ruan and J. O. Winter, *Nano Lett.*, 2011, **11**, 941-945.

13. G. Ruan, G. Vieira, T. Henighan, A. R. Chen, D. Thakur, R. Sooryakumar and J. O. Winter, *Nano Lett.*, 2010, **10**, 2220-2224.
14. K. H. Lee, G. Yang, B. E. Wyslouzil and J. O. Winter, *ACS Applied Polymer Materials*, 2019, **1**, 691-700.
15. G. Hermanson, *Bioconjugate Techniques*, 2013.
16. E. Meijering, O. Dzyubachyk and I. Smal, *Methods Enzymol.*, 2012, **504**, 183-200.
17. A. D. Duong, G. Ruan, K. Mahajan, J. O. Winter and B. E. Wyslouzil, *Langmuir*, 2014, **30**, 3939-3948.
18. M. H. Wong, R. P. Misra, J. P. Giraldo, S. Y. Kwak, Y. Son, M. P. Landry, J. W. Swan, D. Blankschtein and M. S. Strano, *Nano Lett*, 2016, **16**, 1161-1172.
19. G. Vieira, T. Henighan, A. Chen, A. J. Hauser, F. Y. Yang, J. J. Chalmers and R. Sooryakumar, *Phys. Rev. Lett.*, 2009, **103**, 128101.
20. S. Schrittwieser, B. Pelaz, W. J. Parak, S. Lentijo-Mozo, K. Soulantica, J. Dieckhoff, F. Ludwig, A. Guenther, A. Tschöpe and J. Schotter, *Sensors*, 2016, **16**, 828.
21. M. Stanisavljevic, S. Krizkova, M. Vaculovicova, R. Kizek and V. Adam, *Biosens. Bioelectron.*, 2015, **74**, 562-574.
22. K. C. Neuman and A. Nagy, *Nat. Methods*, 2008, **5**, 491-505.
23. R. A. Bissell;, E. Córdova;, A. E. Kaifer; and J. F. Stoddart, *Nature*, 1994, **369**, 133-137.
24. S. J. Rosenthal, J. C. Chang, O. Kovtun, J. R. McBride and I. D. Tomlinson, *Chem Biol*, 2011, **18**, 10-24.
25. G. K. Geiss, R. E. Bumgarner, B. Birditt, T. Dahl, N. Dowidar, D. L. Dunaway, H. P. Fell, S. Ferree, R. D. George, T. Grogan, J. J. James, M. Maysuria, J. D. Mitton, P. Oliveri, J. L. Osborn, T. Peng, A. L. Ratcliffe, P. J. Webster, E. H. Davidson, L. Hood and K. Dimitrov, *Nat Biotechnol*, 2008, **26**, 317-325.